THE ASTRONOMICAL JOURNAL VOLUME 105, NUMBER 1 JANUARY 1993

A SPATIALLY RESOLVED PHOTODISSOCIATION REGION IN THE PLANETARY NEBULA NGC 7027

JAMES R. GRAHAM[1]

Astronomy Department, University of California, Berkeley, California 94720 and Palomar Observatory, California Institute of Technology, Pasadena, California 91125

E. SERABYN

Caltech 320-47, Pasadena, California 91125

T. M. HERBST

Cornell University, Ithaca, New York 14853 and Max-Plank Institute für Astronomie, Königstuhl 17, D-6900 Heidelberg 1, Germany

K. MATTHEWS, G. NEUGEBAUER, AND B. T. SOIFER

Palomar Observatory, California Institute of Technology, Pasadena, California 91125

T. D. WILSON

Palomar Observatory, California Institute of Technology, Pasadena, California 91125 and Department of Physics and Astronomy, University of Rochester, Rochester, New York 14627-0011

S. BECKWITH

Cornell University, Ithaca, New York 14853 and Max-Plank Institute für Astronomie, Königstuhl 17, D-6900 Heidelberg 1, Germany

Received 23 July 1992; revised 14 September 1992

ABSTRACT

High spatial resolution, narrow band, infrared line images and CO (1−0) mm interferometer data are presented for NGC 7027. These data trace emission from the central H II region (Brα), the intermediate photodissociation region [H_2 1−0 S(1) and 3.3 μm dust feature], and the molecular circumstellar envelope [CO (1−0)]. The H II region lies in a cavity in the CO envelope, and consists of a smooth elliptical shell. A striking change of morphology is seen in the H_2 emission and the dust feature. The H_2 1−0 S(1) emission is composed of two components: (1) an incomplete elliptical ring of knots which bounds the ionized gas; (2) a remarkable thin shell which loops around the H II region with fourfold symmetry. The dust emission is similar to that from the ionized gas, but is displaced further from the center, and extends at low surface brightness into four "ears" which fill in the bays delineated by the outermost loops of H_2 emission. No 3.3 μm emission is detectable beyond the outer H_2 shell. The outer loops of H_2 emission and the 3.3 μm emission occupy the region between the edge of the H II region and the inner edge of the molecular gas. It is natural to ascribe the morphology of NGC 7027 to a photodissociation region which separates the ionized and molecular gas. If this is correct then the exterior H_2 loops are due to molecular gas heated by the far-UV emission escaping from the H II region, and delineate a photodissociation front. The H_2 and CO kinematics rule out shock excitation of the H_2 emission and favor UV excitation.

1. INTRODUCTION

The young planetary nebula NGC 7027 is remarkable on account of its association with a substantial circumstellar molecular envelope (Mufson, *et al.* 1975). The presence of such a significant envelope, which is probably the remnant of a cool, slow, wind from the progenitor red giant, is unique, and NGC 7027 therefore presents an important opportunity to study the interaction of the newly formed H II region with the circumstellar material. This interaction takes two forms, namely a mechanical interaction in which a fast wind from the central star ploughs into the slowly moving red giant wind and determines the shape of the resultant planetary nebula (e.g., Kahn & West 1985; Balick *et al.* 1987), and a radiative interaction, where far-ultraviolet radiation (6 eV $< h\nu <$ 13.6 eV) emerges from the H II region and dissociates and heats surrounding molecular gas.

This paper describes new high angular resolution infrared line imaging and mm-wave interferometry of NGC 7027 which trace this interaction. The infrared data consist of images of 2.122 μm H_2 emission, the 3.28 μm dust feature and Brα. Emission from H_2 was discovered in NGC 7027 by Treffers *et al.* (1976). Beckwith *et al.* (1980) demonstrated that the H_2 emission was from molecules which are outside the ionized gas. Gatley *et al.*

[1]Alfred P. Sloan Research Fellow.

 0004-6256/93/010250-08$00.90

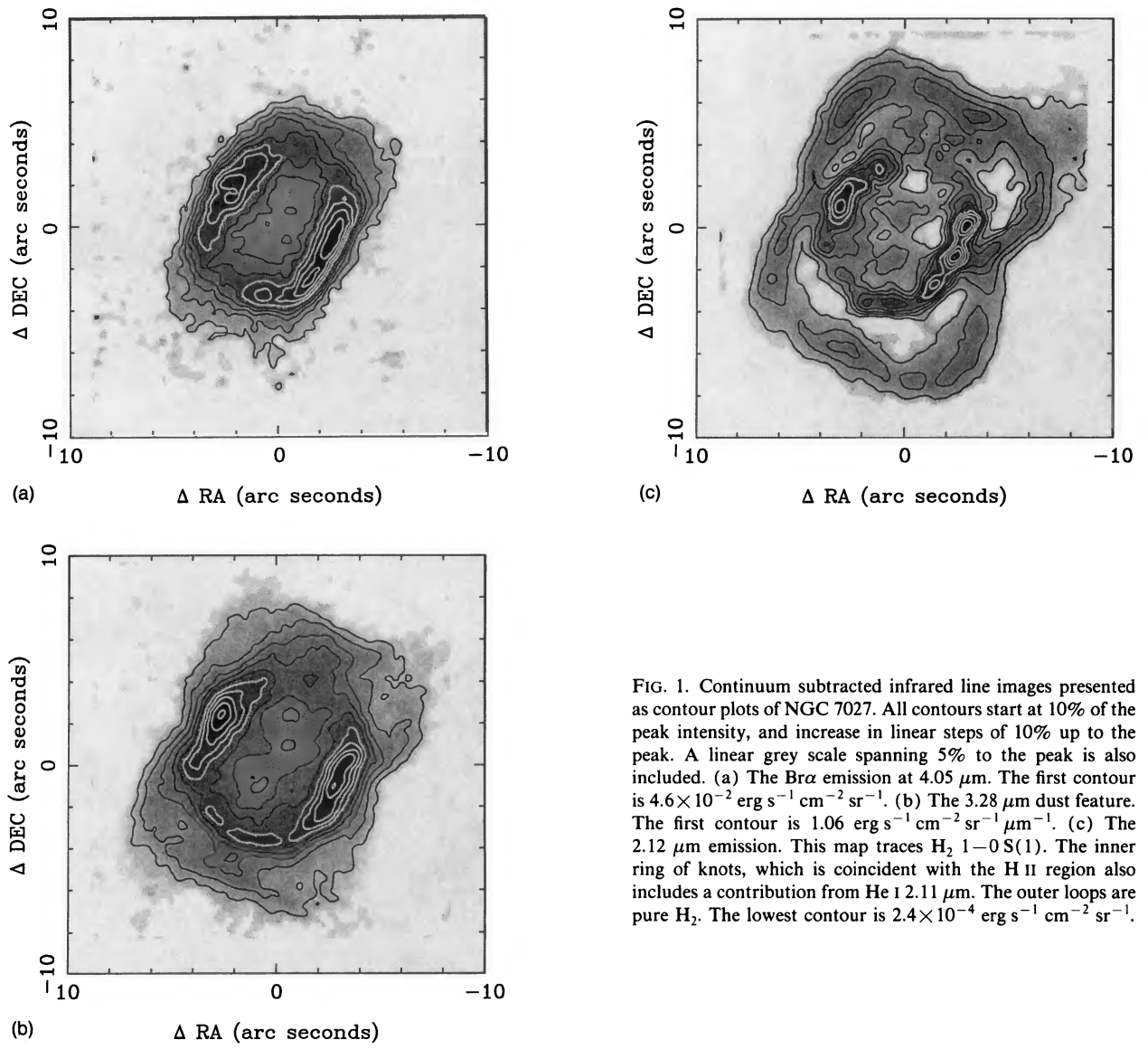

FIG. 1. Continuum subtracted infrared line images presented as contour plots of NGC 7027. All contours start at 10% of the peak intensity, and increase in linear steps of 10% up to the peak. A linear grey scale spanning 5% to the peak is also included. (a) The Brα emission at 4.05 μm. The first contour is 4.6×10^{-2} erg s^{-1} cm^{-2} sr^{-1}. (b) The 3.28 μm dust feature. The first contour is 1.06 erg s^{-1} cm^{-2} sr^{-1} μm^{-1}. (c) The 2.12 μm emission. This map traces H_2 1−0 S(1). The inner ring of knots, which is coincident with the H II region also includes a contribution from He I 2.11 μm. The outer loops are pure H_2. The lowest contour is 2.4×10^{-4} erg s^{-1} cm^{-2} sr^{-1}.

(1988) presented the first H_2 line emission image of NGC 7027. Images of the dust feature emission and Brα are presented by Woodward *et al.* (1989, 1992). A preliminary discussion of the current infrared data appears in Graham *et al.* (1990). The 3.28 μm dust feature was discovered by Merrill *et al.* (1975). Images of this emission have been presented by Woodward *et al.* (1989, 1992). Interferometer CO (1−0) maps of NGC 7027 have been presented by Masson *et al.* (1985) and Bieging *et al.* (1991).

2. OBSERVATIONS

Observations of NGC 7027 were made at the Cassegrain focus of the Hale 200 inch telescope with an infrared camera equipped with a Santa Barbara Research Corporation InSb 58×62 detector array. The pixels project to 0".31 ×0".31 on the sky. The camera is equipped with circular variable filters (CVF) which allow narrow band imaging in the 2 and 3 μm windows at $\Delta\lambda/\lambda\simeq1.3\%$. Observations in the 2 μm window included the lines H_2 1−0 S(1) 2.122 μm and continua at 2.09 and 2.19 μm. The 3 μm observations consist of five CVF setting centered about the 3.3 μm dust feature, and four positions around Brα 4.051 μm. Continuum subtracted line images are presented in Fig. 1. The angular resolution is $\simeq$0".8. The magnitude calibration was determined from observation of standard stars from Elias *et al.* (1982). The magnitudes were converted to flux densities using stellar models and absolute visual measurements of α Lyr (Oke & Schild 1970)

Aperture synthesis observations of CO (1−0) at 115 GHz were made using the Owens Valley Millimeter Array.[2] Five telescope configurations were used, with baselines as long as 200 m east–west, and 140 m north–south. The synthesized beamwidth was 2".8. The shortest projected baseline was 8.3 m, implying that emission structures of scales $\simeq$30" or larger are resolved out. Consequently, 70% of the total CO flux is missing from these data. The 32×1 MHz filter bank provides a velocity resolution of 2.6 over 83 km s^{-1} at 115 GHz. Based on lower

[2]The Owens Valley Radio Observatory is operated by the California Institute of Technology, with support from the National Science Foundation.

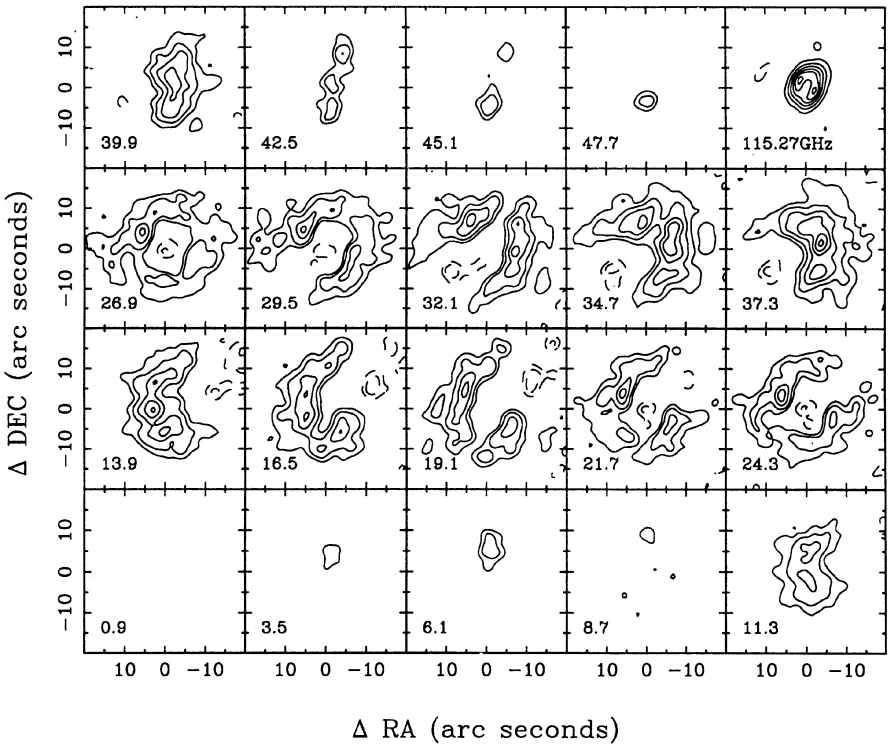

FIG. 2. Interferometer CO (1−0) channel maps of NGC 7027. The maps are continuum subtracted. The number at the lower left of each panel is v_{LSR} in km s^{-1} for that channel. The contour levels are −0.8, −0.4, 0.4, 0.8, 1.6, 2.4, 3.2, and 4.0 Jy/beam. Negative contours are dashed. The last panel shows the 115.27 GHz continuum map. The contours are −0.08, 0.08, 0.20, 0.35, 0.50, 0.62, and 0.74 Jy/beam. The synthesized beamwidth is 2".8. The map center is RA 21 5 9.57 DEC 42 2 2.8 (1950.0).

sideband measurements, the continuum flux integrated over the H II region is 4.6 Jy, in good agreement with the earlier measurement of Masson *et al.* (1985). The resultant continuum subtracted channel maps are shown in Fig. 2.

3. RESULTS

3.1 Infrared Images

The Brα emission, presented in Fig. 1(a), is composed of a smooth elliptical shell with a minor axis diameter of 6". The intensity is peaked at two symmetrical points along the minor axis, and is very similar to the free–free emission mapped at cm wavelengths (Masson 1989). At low surface brightness levels ansae extend from the north–west, south–east, and possibly to the south, confirming structure in the 6 cm map. The current Brα data are in good agreement with the observations of Woodward *et al.* (1989).

The dust feature image at 3.28 μm [Fig. 1(b)] is, at first sight, rather similar to the emission from the H II region [Fig. 1(a)]. However, the radius of the prominent central shell is clearly larger than the H II region (cf. Woodward *et al.* 1989). Low surface brightness emission extends well beyond the edge of the H II region. There is some degree ($\lesssim$5%) of limb brightening of this faint emission, particularly at the position adjacent to the southern end of the H II region. The emission has a sharp outer edge with the possible exception of the "blow out" to the north–west where the faint emission extends to the edge of the image.

The 2.12 μm morphology is quite remarkable [Fig. 1(c)]. It consists of two components: (1) an incomplete elliptical ring of knots which bounds the ionized gas; (2) a thin shell at a greater radius, which loops around the H II region with fourfold symmetry at a maximum diameter of 14". The central ring of knots is almost exactly coincident with the Brα emission from the H II region—the east and west limbs are displaced only $\simeq$0".2 further from the center of the nebula than the Brα emission. The two brightest 2.12 μm knots, on the west limb, straddle the Brα peak.

The bandpass of the 2.12 μm image was centered on the H_2 1−0 S(1) line. In the H II region this image includes H_2 1−0 S(1) and He I $^3P-^3S$ 2.114 μm. High resolution spectroscopy shows that within the H II region the He I line accounts for 20% of the flux in our bandpass (Smith *et al.* 1981). Thus, most of the emission at 2.12 μm within the H II region must be due to H_2 1−0 S(1). Nonetheless, the 2.12 μm CVF image cannot tell whether the central knots are H_2 or He I emission. This ambiguity is resolved by images of NGC 7027 obtained using the infrared camera in tandem with a Fabry-Perot at $\lambda/\Delta\lambda=3000$ (Herbst & Beckwith 1988). These Fabry-Perot data resolve the H_2 and He I lines and show the H_2 emission in the H II region, and reveal that the brightest knots on the east and west

limbs of the H II region are indeed knots of H_2 emission. Consequently, we infer that He I 2.114 μm is smooth like Brα. This is not surprising because Hα and He I 5876 Å images of other planetary nebulae are similar (e.g., Aller 1984). The Fabry-Perot observations and unpublished long slit spectroscopy with the grism installed in the infrared camera show that, as expected, the outer loops of emission beyond the H II region are entirely due to H_2 emission. Most of the H_2 flux ($\simeq$80%) comes from these outer loops—in accord with Beckwith *et al.* (1980) who modeled the H_2 emission as a thin shell with a diameter of 12″.

In Fig. 3 (Plate 7) the three infrared images have been combined into a three-color image to permit comparison of their spatial extend. Figure 3 shows the dust emission extends well beyond the H II region, and that it is bounded by the H_2 emission. The south–east "ear" is clearly filled in with dust emission, while the others are fainter. The overlap of the H_2 and dust in the outer regions is particularly interesting. In some places the H_2 emission and dust are coextensive (i.e., cyan) all the way to the edge of the nebula, for example to the west near the minor axis, and particularly to the north at the major axis. However, there are other locations where the dust emission is relatively weak compared to the H_2 e.g., the south–west loop.

3.2 Millimeter Maps

The CO(1−0) maps in Fig. 2 show a high degree of symmetry in agreement with the results of previous mm observations (Masson *et al.* 1985; Bieging *et al.* 1991). The redshifted, v_{LSR}=29.5–40 km s^{-1}, and blueshifted material, v_{LSR}=11.3–24.3 km s^{-1}, form incomplete arcs displaced to the northeast and southwest of the H II region, respectively. These arcs are shown most clearly in Fig. 4, which displays the emission integrated from v_{LSR}=11.3–40 km s^{-1}. The integrated emission is dominated by two lobes which lie along the minor axis of the H II region at a distance of 7″ from the center of the nebula. This figure emphasizes the axial symmetry of the CO distribution.

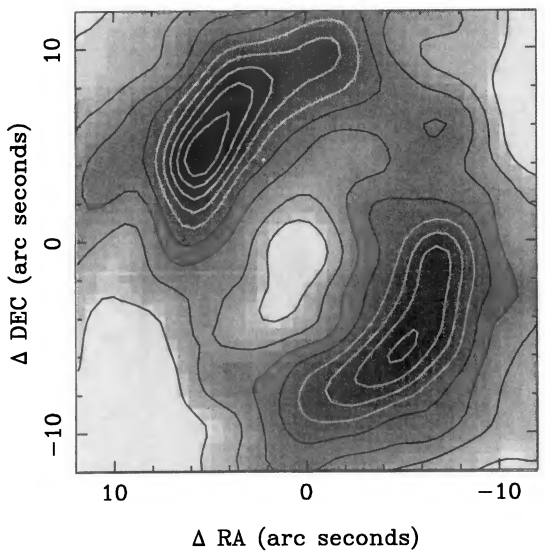

FIG. 4. The integrated CO (1−0) emission from v_{LSR} =11.3–40 km s^{-1} for NGC 7027. The integrated emission consists of two lobes which lie along the minor axis of the H II region at a distance of 7″ from the center of the nebula. Contours run from 10% of peak in linear intervals of 10% to the peak. The lowest contour corresponds to an average flux per channel of 0.19 Jy/beam. The synthesized beamwidth is 2″.8. The data are also displayed as a linear greyscale covering the same data range.

4. DISCUSSION

4.1 CO Kinematics

The CO channel maps contain information regarding the kinematics of the molecular envelope of NGC 7027, but this information is rather difficult to extract directly from these maps. Therefore, we present position–velocity diagrams for the major and minor axis of the CO cloud in Fig. 5. These diagrams are useful because they provide a summary of the kinematic information. The minor axis lies at a position angle (PA) of 65°, passing through the northeast and southwest CO lobes adjacent to the H II region. This axis is approximately parallel to the PA of the minor axis of the H II region (60°; Masson 1986).

Figures 5(a) and 5(b) show a ring of emission characteristic of a resolved expanding shell. The most noteworthy aspect of these plots is the large velocity gradients at offsets of ±8″. This abrupt change in velocity leads to a locus of maximum emission which is distinctly box shaped. These figures also emphasize the clumpiness of emission seen in the channel maps and demonstrate that it is also present in the velocity domain, suggesting that the clumps correspond to genuine three-dimensional structures. However, the minor axis plot shows that the two dominant CO lobes seen in the central velocity channel map are part of an equatorial ring which forms a large, relatively coherent, structure. This is in contrast to the major axis emission distribution which is more fragmented.

Quantitative information regarding the kinematics of NGC 7027 can be found by comparing the position velocity plots with a model consisting of an expanding, optically and geometrically thin, triaxial ellipsoidal shell. This model is similar to those proposed for the H II region (e.g., Atherton *et al.* 1979; Masson 1986; Roelfsema *et al.* 1991). Expansion laws of $v \propto r^{\alpha}$, with $\alpha = -1$, 0, and 1 were considered. In all cases the expansion was assumed to be radial. As the model has a large number of free parameters—the axes' lengths, the expansion velocity, α, and the inclination—formal least-squares fitting was not performed. Rather, position velocity plots for a large range of parameters were calculated and compared by eye with the observations. The first deduction from this exercise is that only uniformly expanding models (α=0) can account for the "boxy" shape of the locus of maximum emission. Homologous expansion (α=1) predicts ellipsoidal position velocity plots, which are inconsistent with the long straight sections seen in Figs. 5(a) and 5(b). On the other hand $\alpha = -1$ predicts position velocity plots with cusps and concave sections which are not seen.

Uniform radial expansion of a prolate spheroid, inclined to the line of sight, leads to a velocity field which is consistent with the observed position velocity diagrams. For a

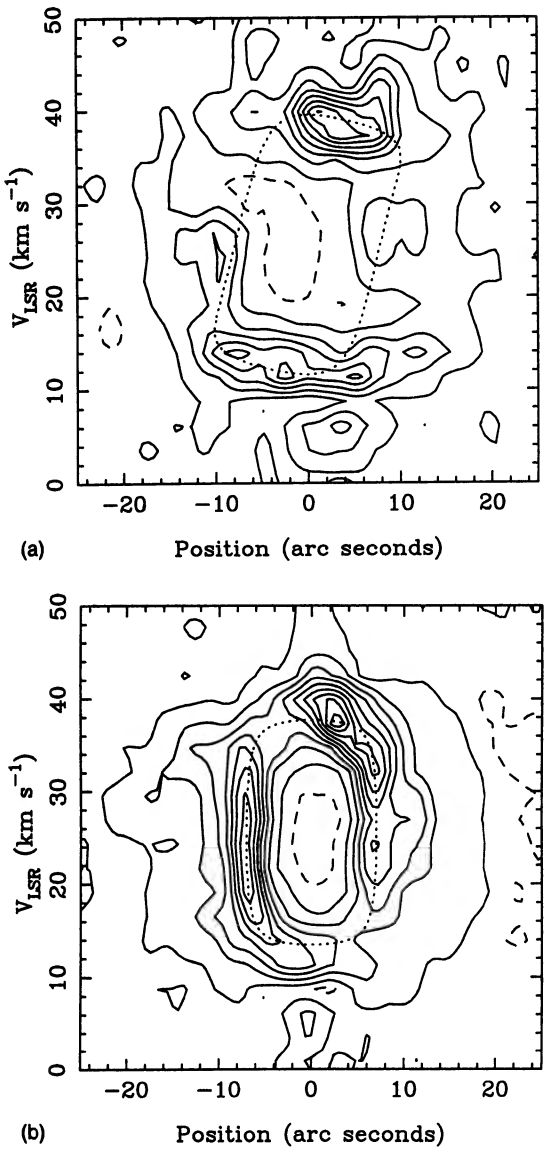

FIG. 5. (a) is the major axis (PA 155°) position velocity plot of the CO (1−0) data. (b) is the minor axis (PA 65°) position velocity plot. Note the distinctly box-shaped contours which are characteristic of a uniformly expanding prolate ellipsoidal shell. In both plots the dotted line shows the locus of emission from a thin uniformly expanding shell. See Table 1 for the model parameters.

radial flow, the expansion velocity can be determined directly from the separation of the emission peaks along the major axis. The minor axis dimension is the diameter of the ring at the central velocity. The ratio of the extreme velocities in the major and minor axis plots gives the inclination angle. A uniform expansion model, with parameters which are listed in Table 1, is compared with the observations in Figs. 5(a) and 6(b). It is clear from this comparison that the model provides a good explanation for the kinematic data, and a thin shell can account for a substantial fraction of the observed CO emission.

Better agreement could undoubtedly be achieved by a model consisting of a thick shell with some velocity dispersion. As the CO (1−0) optical depth probably approaches unity along some lines of sight (Jaminet *et al.* 1991), a more complete model should also include radiative transfer effects.

TABLE 1. Kinematic model of the CO shell.

Inclination of major axis to the line of sight	60°
Major axis radius	16″
Minor axis radius	7″
Systemic velocity (LSR)	25.6 km s^{-1}
Expansion velocity	14 km s^{-1}

4.2 Comparison of Infrared and mm Maps

Figure 6 shows an overlay of the H_2 and CO at the systemic velocity. The correlation between the H_2 and CO emission in the figure is striking. The inner ring and outer loops of H_2 sit in the central CO cavity. Within the limits of the resolution of the CO data the lowest CO contour delineates the outer boundary of the H_2. The maxima in the CO along the minor axis are aligned with the indentations in the outer H_2 shell along this direction. The secondary pair of CO peaks, to the north and south, are associated with the pinching in of the H_2 shell along the major axis. However there is an offset of $\simeq 35°$ between the axes joining the secondary CO peaks and the H_2 indentation along the major axis. The "blowout" seen in faint H_2 emission to the north–west lies along the axis with least CO emission.

Several studies of NGC 7027 show that the CO (1−0) is not very optically thick, i.e., $\tau(1-0) \lesssim 1$, and the intensity is approximately proportional to column density (Deguchi *et al.* 1990; Jaminet *et al.* 1991). Thus, CO maps reveal the density structure of the circumstellar molecular gas. If the kinematic model of Sec. *4.1* is correct, then the

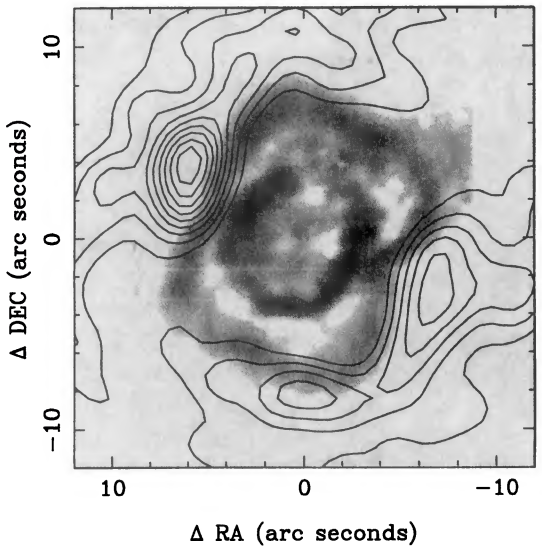

FIG. 6. Contours of CO (1−0) emission at $v_{LSR}=25.6$ km s^{-1}, which corresponds to the central velocity. The contours are linear starting 10% of peak and increasing in steps of 10%. The lowest contour is 0.5 Jy/beam. This figure also shows the H_2 emission displayed as a greyscale. The display corresponds to a linear stretch from 10% to maximum.

central channel map corresponds to a planar slice perpendicular to the line of sight through the center of the shell, and this channel should show the envelope in cross section giving the most unambiguous measure of the structure of the molecular envelope free from projection effects.

The current CO distribution reflects the original spatial distribution of the ejected material and its subsequent modification by the central star. A fast wind from the star forms a bubble of hot, high pressure gas which sweeps up the previous ejecta into a thin shell (*e.g.*, Kahn 1983). If the shock driven by the expanding bubble is fast enough ($v_s \gtrsim 25$–45 km s^{-1}; Kwan 1977; Draine *et al.* 1983) then the swept-up molecular gas is completely dissociated. Ionizing radiation from the star forms an H II region which expands behind an ionization front. Far-UV radiation (6 eV $< h\nu <$ 13.6 eV) can escape from the H II region. Since this radiation can dissociate H_2, a photodissociation front precedes the ionization front. Shocks and UV light can vibrationally excite H_2. Thus the remarkable correlation seen between CO and H_2 in Fig. 6 arises because the outer H_2 loops delineate either a shock or a photodissociation front propagating into the molecular envelope. In general, both a shock and a photodissociation region will surround the H II region. We discuss our observations with the goal of deciding which is responsible for the observed infrared emission.

4.3 The Origin of the CO Kinematics

At first sight the kinematic model appears contrived because the ellipsoidal shell at different distances from the central star expands at the same speed. This might suggest that the gas along the poles of the nebula must have decelerated in order to reach a greater distance from the star, yet currently be moving at the same velocity. Implicit in this is the assumption that the CO which forms the shell was ejected at a single epoch. A much more likely picture is that the CO originally formed a thick uniformly expanding shell. Interaction with the H II region then eroded the molecular shell. If the density is lower along one axis, then the cavity will increase in size faster in this direction. The net result is a prolate ellipsoidal shell with the same velocity along the major and minor axes.

4.4 Shock Excitation

Several observations suggest supersonic motions are present in the molecular envelope of NGC 7027. Therefore, it is important to investigate the role of shocks in determining the observed morphology at infrared and mm wavelengths. However, we anticipate the conclusion of this and the following section by stating that shocks are probably not responsible for exciting the H_2 emission or its relationship to the CO.

Figure 6 shows that the morphology of the central CO cavity does not match the H II region, but rather the outer H_2 loops. This can be explained if a dissociative shock propagates ahead of the ionization front into the molecular gas. The dereddened average surface brightness of the H_2 1−0 S(1) emission in the loops is $\simeq 8\times10^{-4}$ erg s^{-1} cm^{-2} sr^{-1}, assuming $A_K = 0.34$ mag (Woodward *et al.* 1992). For a density in the equatorial plane of $n_{H_2} \simeq 3 \times 10^4$ cm^{-3} (Jaminet *et al.* 1991) a shock velocity of $v_s \simeq 25$ km s^{-1} is required (Draine *et al.* 1983). There is no observational evidence for such fast shocks in NGC 7027.

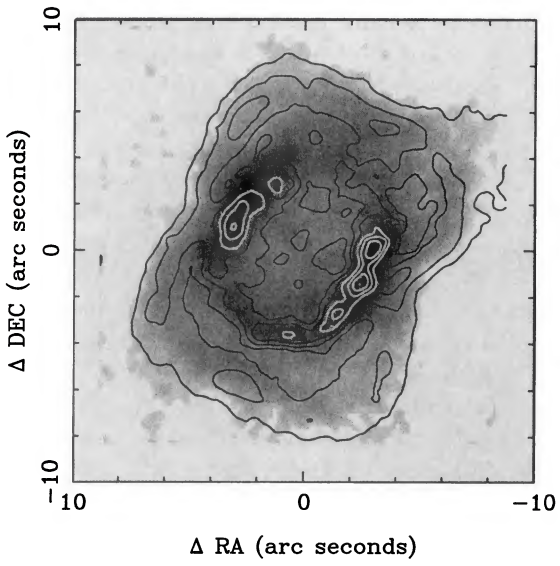

FIG. 7. Comparison of the 3.3 μm dust feature, displayed as a greyscale, with contours of H_2 emission. The 3.3 μm dust emission is bounded by the H_2, providing compelling evidence that the outer H_2 loops delineate a photodissociation front.

The highest velocity CO (1−0) emission is observed at $v_{LSR} = 3.5$ and 47.7 km s^{-1}, i.e., $\Delta v \simeq \pm 22.5$ km s^{-1} (cf. Fig. 2). This emission is located close to the edge of the H II region at its northern and southern ends. Masson *et al.* (1985) also reported high velocity emission towards the center of the nebula, and attributed it to a layer of shock accelerated neutral gas surrounding the H II region. The similarity of the expansion speed of the high velocity CO and the ionized gas (23 km s^{-1}, e.g., Roelfsema *et al.* 1991), suggests that the surrounding molecular gas has been shock accelerated by the expansion of the H II region (cf. Jaminet 1991). The resulting shock speed is $v_s \simeq 8.5$ km s^{-1} for the isothermal case, given the observed expansion speeds of the ionized and molecular gas. The principal coolants of slow shocks ($v_s < 15$ km s^{-1}) in dense molecular gas ($n_H = 10^4$–10^6 cm^{-3}) are pure rotational lines of H_2 and [O I] fine structure lines (Draine *et al.* 1983; McKee *et al.* 1984). Consequently, the molecular shock in the envelope of NGC 7027 is too slow to produce observable 1−0 S(1) emission. The kinematics of the H_2 emission, discussed in Sec. *4.5*, confirm this conclusion.

4.5 A Photodissociation Region Surrounding NGC 7027

An alternative explanation for the cavity in the CO shell and the close correlation with the outer H_2 loops is that the H_2 emission comes from radiatively heated gas in a photodissociation region. The thin, limb brightened H_2 morphology is consistent with emission from a photodissociation

region (Tielens & Hollenbach 1985). Figure 7 compares the 3.3 μm dust feature with the H_2 emission and shows that they are coextensive outside the H II region. (See also Fig. 3.) The 3.3 μm dust feature usually delineates the interfaces between ionized and molecular gas (e.g., Sellgren *et al.* 1990). Therefore, this figure provides compelling evidence for a photodissociation region between the ionized gas and the inner edge of the CO cavity.

Far-UV radiation excites both H_2 and 3.3 μm dust emission. The excitation of these species occurs in distinct parts of the photodissociation region, and the emission should have a distinctive morphology. The photodissociation front is located at a distance equivalent to $A_V = 1$–2 mag into the neutral cloud, and corresponds to the penetration depth of far-UV light (Tielens & Hollenbach 1985). The exact position depends upon the relative importance of dust extinction and molecule self shielding. The H_2 is collisionally excited in UV heated gas; the abundance of vibrationally excited H_2 is sharply peaked at the photodissociation front (Tielens & Hollenbach 1985; Burton *et al.* 1990). The 3.3 μm feature is due to the fundamental C—H stretch mode of hydrogenated bonds on carbon molecules such as polycyclic aromatic hydrocarbons (e.g., Puget & Leger 1989). The 3.3 μm emission is fluorescently excited by far-UV light and therefore traces the penetration of this radiation into the gas surrounding the H II region. Figures 3 and 7 show that the 3.3 μm dust emission extends well beyond the edge of the H II region, but that it is bounded by the outer loops of H_2 emission. This is precisely the morphology expected for a photodissociation front where the propagation of far-UV light is determined by dust extinction.

The size of the gap between the H II region and the CO is correct for a photodissociation region assuming that attenuation of far-UV is dominated by dust and standard extinction—$N_H = 1.6 \times 10^{21} A_V$ cm^{-2}. The minor axis dimensions of the H II region and the CO shell are 3″ and 7″, respectively. Thus, the width of the photodissociation region is $\simeq 4''$. At a distance of 880 pc and with $n_{H_2} = 3 \times 10^4$ cm^{-3}, the column in the photodissociation region is $\simeq 3 \times 10^{21}$ cm^{-2}. This column of gas corresponds to $A_V = 1.8$ mag, and falls within the expected range of 1–2 mag. The larger size of the CO shell along the major axis presumably indicates a corresponding lower density in this direction.

The observed H_2 surface brightness is similar to that expected for the physical conditions in NGC 7027 according to photodissociation region models (cf. Black & Van Dishoeck 1987; Burton *et al.* 1990). If the density in the equatorial plane at the edge of the H II region is $n_{H_2} \simeq 3 \times 10^4$ cm^{-3} and the far-UV radiation field is 2×10^3 times the interstellar field at a radius of 7″ (Black & van Dishoeck 1987) then $I_{1-0S(1)} = 5.5 \times 10^{-5}$ erg s^{-1} cm^{-2} sr^{-1} (Sternberg 1988). Models of photodissociation regions show that the vibrationally excited H_2 emission comes from a region $\delta R/R \simeq 0.1$ (Tielens & Hollenbach 1985). The limb brightening factor for a spherical shell of radius R, and thickness δR, is $2(2R/\delta R)^{0.5}$. Therefore, the peak 1−0 S(1) surface brightness excited by far-UV radiation should be 4.9×10^{-4} erg s^{-1} cm^{-2} sr^{-1}, or about 60% of the typical observed H_2 surface brightness. The calculated surface brightness depends on uncertain properties of the circumstellar shell, such as the gas temperature, the gas-to-dust ratio, the optical properties of the dust grains, and the details of the surface chemistry which lead to formation of H_2. For example, different grain models lead to fluxes which vary by a factor of about 3 (Black & Van Dishoeck 1987). Consequently, the measured infrared H_2 flux is in accord with that calculated for the photodissociation region model.

CO observations imply that the density is comparable to the critical density ($n_{H_2}^{crit} \simeq 10^4$ cm^{-3}) for thermalization of the lower ($v \lesssim 2$) vibrational levels of H_2. Therefore, measurement of the relative intensity of $v = 1-0$ and $v = 2-1$ transitions cannot be used as an unambiguous diagnostic for UV heating (Sternberg & Dolgarno 1989). On the other hand, the H_2 rotation and vibrational populations in NGC 7027 are not in LTE. This observation lead Tanaka *et al.* (1989) to decompose the H_2 emission into a mixture of thermal and fluorescent components. As Tanaka *et al.* point out, the thermal component does not necessarily mean shocked gas. The presence of both components is qualitatively consistent with emission from a dense photodissociation region. The detection of [C II] 158 μm emission for NGC 7027 is also consistent with the photodissociation region interpretation (Genzel *et al.* 1988).

Shock excited and photodissociation region H_2 emission have distinct kinematic signatures. Emission from a photodissociation region is found at the rest velocity of the illuminated gas, while shock excited emission comes from accelerated gas and therefore is seen at a different velocity from the ambient, unshocked material. For an isothermal shock the velocity difference is equal to the shock velocity (Spitzer 1978). A high resolution spectrum of the 1−0S(1) emission from NGC 7027, in a small beam passing through the center of the nebula, shows a double peaked profile characteristic of an expanding shell (Geballe 1990). The separation of the peaks corresponds to an expansion velocity of 15 km s^{-1}. There is none of the high velocity molecular gas ($\delta v = \pm 40$ km s^{-1}) which would be present if the H_2 emission were shock excited. On the contrary, the H_2 shell is expanding at essentially the same speed as the CO shell. Therefore, the simplest interpretation is that the bulk of the H_2 emission comes from unshocked gas which is part of a photodissociation region at the inner edge of the CO shell.

4.6 Comparison with the Orion Bar

Similar stratification of ionized gas, dust feature emission and vibrationally excited H_2 is found in the Orion Bar (Sellgren *et al.* 1990), and is one of the reasons for attributing the 3.3 μm and H_2 emission to a photodissociation region. The similarity between the Orion photodissociation region and NGC 7027 is also quantitative because the ratio of peak H_2 and dust surface brightnesses are also comparable: $I_\lambda(3.3\,\mu\text{m})/I_{H_2} = 1700\,\mu\text{m}^{-1}$ in the Orion photodissociation region; $I_\lambda(3.3\ \mu\text{m})/I_{H_2} = 2900\ \mu\text{m}^{-1}$ for NGC 7027.

The main difference between the Orion bar and NGC 7027 is that H_2 and 3.3 μm emitting dust are present in the H II region in NGC 7027. This difference is most likely due to the youth of the ionized region in NGC 7027 [$\simeq$600 yr, Masson (1989)]. PAHs are destroyed and dehydrogenated inside an H II region by the ionizing flux and hot electrons, but the time scale must be longer than the age of NGC 7027. If there has been inadequate time for substantial destruction of PAHs in NGC 7027, then the larger value of $I_\lambda(3.3\ \mu\text{m})/I_{H_2}$ in NGC 7027 may also be due to the youth of the nebula. The presence of the inner ring of H_2 adjacent to the H II is harder to explain. The implication is that some H_2 survives the passage of the photodissociation front. This would point to the presence of dense molecular knots in which H_2 can survive the interval between the arrival of the photodissociation and ionization fronts.

5. CONCLUSIONS

We have presented high resolution infrared and mm line data for the planetary nebula NGC 7027 which allow us to investigate the nature of the transition region between the outer edge of the H II region, and the inner edge of the nebula's molecular envelope. This region is traced by vibrationally excited H_2 emission and the 3.3 μm feature of interstellar dust. The H_2 morphology is particularly striking, and consists of an inner shell of emission adjacent to the H II region, and outer loops which are coincident with the inner edge of the CO shell.

The emission is stratified, with Brα, 3.3 μm dust and H_2 occupying a central cavity in the CO distribution. Both the dust feature and the H_2 emission extend well beyond the edge of the ionized gas and bridge the gap between the edge of the H II region and the inner edge of the molecular gas. The H_2 bounds the 3.3 μm dust emission. This morphology is characteristic of a photodissociation region. The observed H_2 surface brightness is consistent with the emission from far-UV heated molecular gas.

The kinematics of the CO are in accord with emission from a shell expanding uniformly at 14 km s^{-1}. Comparison of the CO observations with Geballe's (1990) high resolution spectrum of the H_2 1$-$0 S(1) line show that the bulk of the H_2 emission comes from gas at the same velocity as the CO shell, i.e., unshocked gas. The CO channel maps show regions of gas shock accelerated by the expansion of the H II region. However, these shocks are too slow to excite observable H_2 emission.

J. R. G. is supported in part by an Alfred P. Sloan Research Fellowship. Infrared astrophysics at Caltech is supported by a grant from the NSF. Observations at Palomar were made as part of a continuing collaborative agreement between Cornell and Caltech. We thank Juan Carrasco, the night assistant at the 200 inch telescope, and the entire staff of Palomar observatory. We acknowledge valuable discussions on photodissociation regions with Xander Tielens.

REFERENCES

Aller, L. H. 1984, Physics of Thermal Gaseous Nebulae (Reidel, Dordrecht)
Atherton, P. D., Hicks, T. R., Reay, N. K., Robinson, G. J., & Worswick, S. P. 1979, ApJ, 232, 786
Balick, B., Preston, H. L., & Icke, V. 1987, AJ, 94, 1641
Beckwith, S., Neugebauer, G., Becklin, E. E., Matthews, K., & Persson, S. E. 1980, AJ, 85, 886
Bieging, J. H., Wilner, D., & Thronson, H. A. 1991, ApJ, 379, 271
Black, J. H., & Van Dishoeck, E. F. 1987, ApJ, 322, 412
Burton, M. G., Hollenbach, D. J., & Tielens, A. G. G. M. 1990, ApJ, 365, 620
Deguchi, S., Izumiura, H., Kaifu, N., Mao, X., Nguyen-Q.-Rieu, & Ukita, N. 1990, ApJ, 351, 522
Draine, B. T., Roberge, W. G., & Dalgarno, A. 1983, ApJ, 264, 485
Elias, J. H., Frogel, J. A., Matthews, K., & Neugebauer, G. 1982, AJ, 87, 1031
Gatley, I. Depoy, D. L. & Fowler, A. M. 1988, Science, 242, 1264
Graham, J. R., Matthews, K., Neugebauer, G., Soifer, B. T., Wilson, T. D., Beckwith, S., & Herbst, T. 1990, BAAS, 22, 813
Geballe, T. R. 1990, in Molecular Astrophysics, edited by T. W. Hartquist (Cambridge University Press, Cambridge), p. 345
Genzel, R., Harris, A. I., & Stutzki, J. 1988, Infrared Spectroscopy in Astronomy, Proceedings of the 22nd ESLAB Symposium, edited by B. H. Kaldeich (ESTEC, Noordwijk, The Netherlands), p. 115
Herbst, T. M., & Beckwith, S. 1988, PASP, 100, 635
Hollenbach, D. J., Takahashi, T., & Tielens, A. G. G. M. 1991, ApJ, 377, 192
Jaminet, P. A., Danchi, W. C., Sutton, E. C., Russell, A. P. G., Sandell, G., Biejing, J. H., & Wilner, D. 1991, ApJ, 380, 461
Kahn, F. D. 1983, in Planetary Nebulae, IAU Symposium No. 103, edited by D. R. Flower (Reidel, Dordrecht), p. 305
Kahn, F. D., & West, K. A. 1985, MNRAS, 212, 837
Kwan, J. 1977, ApJ, 216, 713
Masson, C. R., *et al.* 1985, ApJ, 292, 464
Masson, C. R. 1986, ApJ, 302, L27
Masson, C. R. 1989, ApJ, 336, 294
McKee, C. F., Chernoff, D. F., & Hollenbach, D. J. 1984, in Galactic and ExtraGalactic Infrared Spectroscopy, edited by M. F. Kessler and J. P. Phillps (Reidel, Dordrecht), p. 103
Merrill, K. M., Soifer, B. T., & Russell, R. W. 1975, ApJ, 200, L37
Mufson, S. L., Lyon, J., & Marionni, P. A. 1975, ApJ, 201, L85
Oke, J. B., & Shild, R. E. 1970, ApJ, 161, 1015
Puget, J. L., & Leger, A. 1989, ARA&A, 27, 161
Roelfsema, P. R., Goss, W. M., Pottasch, S. R., & Zijlstra, A. 1991, A&A, 251, 611
Sellgren, K., Tokunaga, A. T., & Nakada, Y. 1990, ApJ, 349, 120
Smith, H. A., Larson, H. P., & Fink, U. 1981, ApJ, 244, 835
Spitzer, L. 1978, in Physical Processes in the Interstellar Medium (Wiley, New York), p. 218
Sternberg, A. 1988, ApJ, 332, 400
Sternberg, A., & Dalgarno, A. 1989, ApJ, 338, 197
Tanaka, M., Hasegawa, T., Hayashi, S. S., Brand, P. W. J. L., & Gatley, I. 1989, ApJ, 336, 207
Tielens, A. G. G. M., & Hollenbach, D. 1985, ApJ, 291, 722
Treffers, R. R., Fink, V., Larson, H. P., & Gautier, T. N. 1976, ApJ, 209, 793
Woodward, C. E., Pipher, J. L., Shure, M., Forrest, W. J., & Sellgren, K. 1989, ApJ, 342, 860
Woodward, C. E., Pipher, J. L., Forrest, W. J., Moneti, A., & Shure, M. A. 1992, ApJ, 385, 567

1993AJ....105..250G

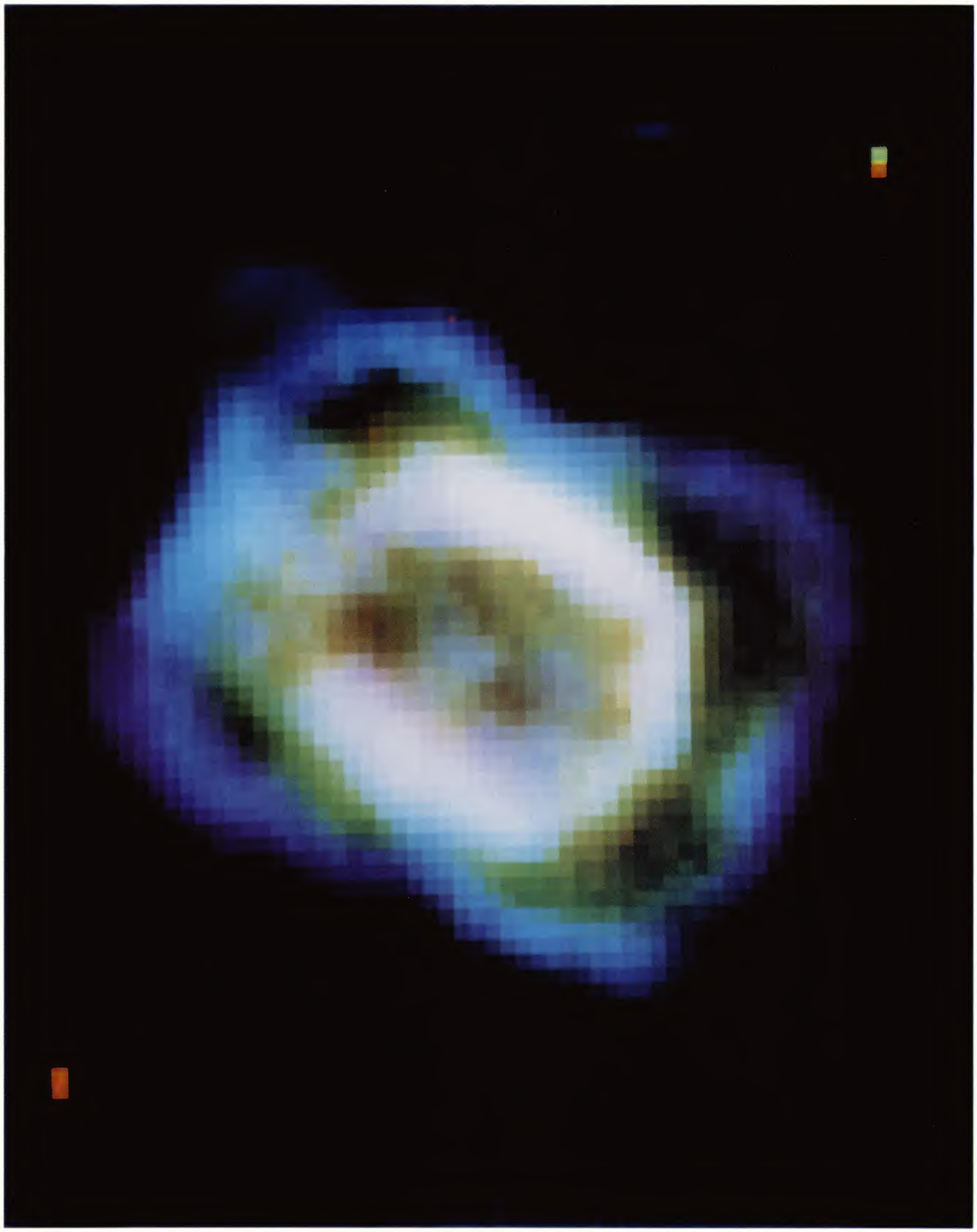

FIG. 3. A three-color composite of the infrared images where red represents Brα, green the dust feature, and blue H_2. The central regions are burned in to emphasize the outer structure. The dust emission extends well beyond the H II region, and shows that it is bounded by the H_2 emission. In some places the outer loops are cyan indicating that the H_2 emission and dust are coextensive all the way to the edge of the nebula, for example to the west near the minor axis, and particularly to the north at the major axis.

Graham *et al.* (see page 253)

THE ASTRONOMICAL JOURNAL

FOUNDED BY B. A. GOULD
1849

VOLUME 105 **January 1993 ~ No. 1644** HARTFORD, CONN. NUMBER 1

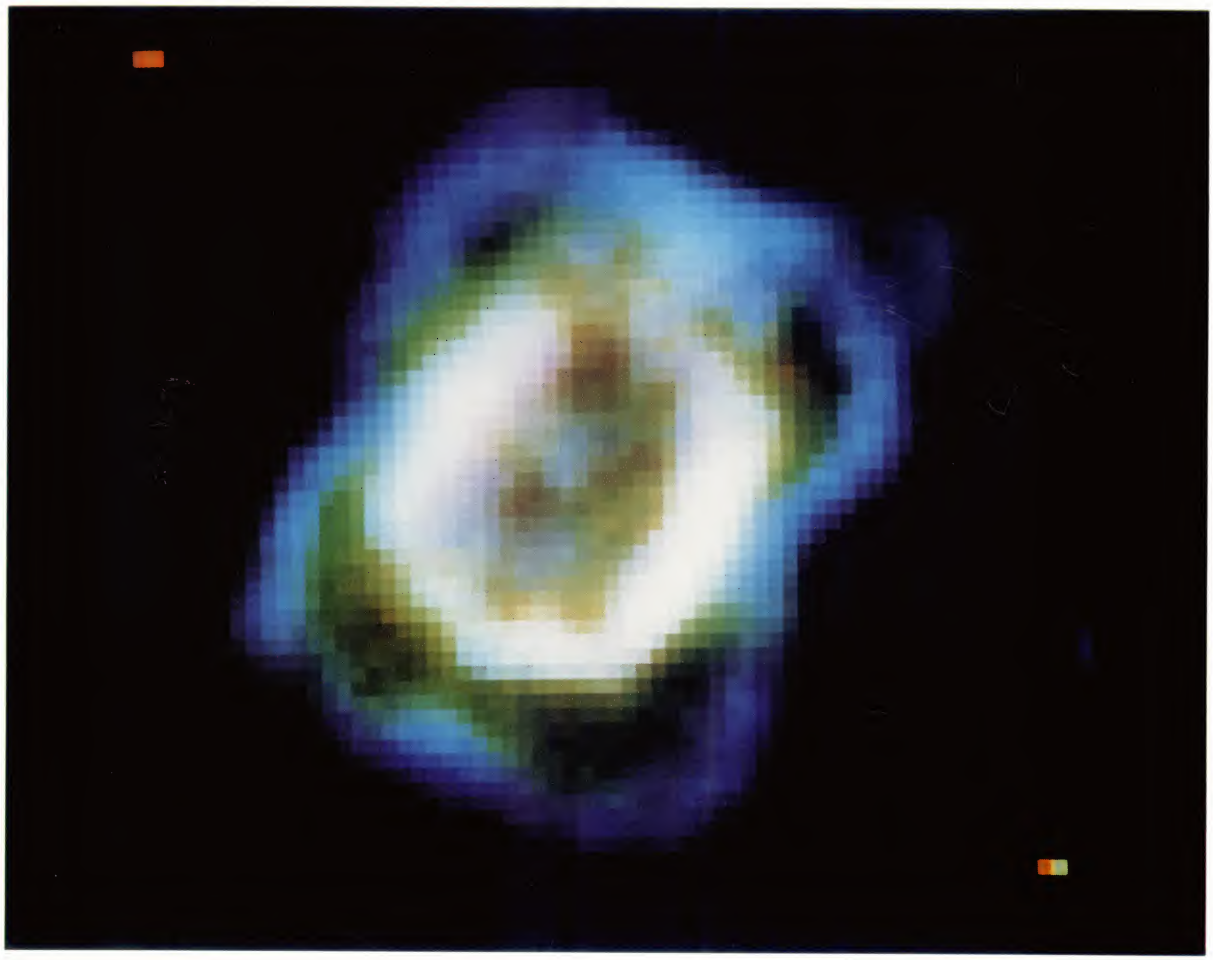

(See Page 250)

Published for the
AMERICAN ASTRONOMICAL SOCIETY
by the
AMERICAN INSTITUTE OF PHYSICS